Impact of Battery Aging on the Performance of Low-Complexity State-of-Charge Estimators: A Real-Data Analysis*

Isaías Valente de Bessa[1], Gildas Besançon[2], Antoneta Iuliana Bratcu[2],
Daniel Coutinho[3], Iulian Munteanu[2,4]

Abstract— **This paper proposes a low-complexity State-of-Charge (SoC) estimation strategy for lithium-ion batteries under aging. The approach reformulates a second-order equivalent circuit model into a higher-order linear time-varying structure, enabling the use of a classical Kalman filter with linear output (KFLO). This avoids both the linearization errors of the EKF and the computational overhead of the UKF. A hybrid identification scheme updates internal resistance online via event-driven current variations while recursively correcting cycle efficiency. Experimental validation on progressively aged cells shows that the estimator maintains robust accuracy, achieving RMSE below 2.5% and MAE below 1.3% even for aged batteries, outperforming EKF and UKF benchmarks. Results demonstrate the method's suitability for resource-constrained BMS applications requiring long-term reliability.**

Index Terms— **low-complexity, State-of-Charge, Kalman filter with linear output, hybrid identification.**

I. Introduction

The increasing integration of renewable sources into the electrical grid demands energy storage systems (ESS), where lithium-ion batteries (LIBs) are predominant due to their high energy density, low self-discharge, and efficiency [1]. Safe and efficient LIB operation requires a Battery Management System (BMS) that estimates internal states such as State-of-Charge (SoC) and State-of-Health (SoH) [2].

Several SoC estimation techniques exist, including state observers [3] and Kalman filters [4]. However, accuracy degrades as batteries age: internal parameters such as resistance and capacity change, compromising estimators designed for fresh cells, especially when using low-complexity ones that rely on simplified models.

Battery aging is typically categorized into two distinct modes: calendar aging and cycling aging [5]. Calendar aging occurs during storage or idle periods, driven by factors such as elevated temperature and self-discharge, which gradually degrade the cell's chemistry even without current flow [6]. In contrast, cycling aging results from the cumulative stress imposed by repeated charge and discharge cycles, being directly influenced by the operating profile such as depth of discharge, charge/discharge rates, and temperature variations [7]. Given that this work utilizes real cycling data to evaluate estimator performance under realistic operating conditions, the effects of cycling aging are of primary interest.

In this work, *low-complexity estimator* means model and algorithmic simplicity. We adopt a second-order equivalent circuit model (ECM) [8], which balances fidelity and computational cost. ECMs confine nonlinearity to the output equation via the open-circuit voltage (OCV) [9], but this still challenges low-complexity observer design. Parameter identification includes offline characterization and online adaptation [10], with the OCV curve being essential for observability [11].

Among estimation strategies, Kalman filtering is well-established. The Extended Kalman Filter (EKF) linearizes the nonlinear output [10], while the Unscented Kalman Filter (UKF) uses sigma-point sampling for improved accuracy [12], despite its higher computational cost. This accuracy/complexity trade-off is critical under aging: EKF linearization errors may increase, while UKF's computational demands may exceed low-complexity constraints.

This trade-off between accuracy and computational cost is particularly relevant when battery aging is considered. As the battery degrades, its internal dynamics become increasingly complex and potentially more nonlinear, which may exacerbate the limitations of linearization-based approaches like the EKF. Conversely, while the UKF might better capture aging-induced nonlinearities, its higher computational demands may be prohibitive for low-complexity implementations.

In this context, this paper proposes a novel low-complexity SoC estimation strategy that addresses both the linearization errors inherent to EKF-based approaches and the computational overhead of sigma-point methods such as the UKF. The proposed estimator uses a second-order ECM, whose nonlinear output characteristic is immersed into a higher-order linear time-varying formulation. This reformulation enables the use of a classical Kalman filter with linear output (KFLO), significantly reducing computational complexity while maintaining a tractable representation of the battery's dynamics.

A key aspect of the proposed approach lies in its hybrid parameter identification strategy. While the RC parameters, OCV characteristic, and battery capacity are identified offline

*This study was financed in part by CAPES ("Coordenação de Aperfeiçoamento de Pessoal de Nível Superior") under grants 88881.878833/2023-01 and 88887.077184/2024-00, CNPq ("Conselho Nacional de Desenvolvimento Científico e Tecnológico") under grants 303289/2022-8/PQ, 441533/2023-0, and 406477/2022-1, and FAPESC ("Fundação de Amparo à Pesquisa e Inovação do Estado de Santa Catarina") under grants 2022TR002110, 2023TR001506, and 2025TR653, and in part by IRGA ("Initiatives de Recherche à Grenoble Alpes") project PaDeSoH ("Partial-differential-equation-based estimation of battery state of health"), in the framework of "Investissement d'avenir" ANR-15-IDEX-02 French national research and innovation funding program.

[1]Graduate Program in Automation and Systems Engineering, Federal University of Santa Catarina, Florianópolis, SC 88040-900 Brazil (e-mail: isaias.bessa@posgrad.ufsc.br)

[2]Univ. Grenoble Alpes, CNRS, Grenoble INP, GIPSA-lab, 38000, Grenoble, France (e-mails: {gildas.besancon,antoneta.bratcu}@gipsa-lab.grenoble-inp.fr)

[3]Departament of Automation and Systems, Federal University of Santa Catarina, Florianópolis, SC 88040-900 (e-mail: daniel.coutinho@ufsc.br)

[4]PRECIS Research Institute, National University of Science and Technology POLITEHNICA Bucharest 313 Splaiul Independenței, Sector 6, Bucharest, RO-060042, Romania (e-mail: iulian.munteanu0108@upb.ro)

— given that their slow-varying nature has limited impact on short-term estimation performance — the internal resistance is updated in real time using an event-driven mechanism triggered by current variations. Additionally, the cycle efficiency is recursively updated online, serving as a corrective factor for the battery's usable capacity during operation.

The paper is structured as follows. Section II presents the ECM and immersion transformation. Section III details the identification framework and KFLO. Section IV discusses experimental results comparing fresh and aged cells. Section V concludes and outlines future work.

II. Battery model

A. Second-order equivalent circuit model

A second-order equivalent circuit model (ECM) is adopted due to its favorable trade-off between accuracy and complexity [13], [14], as shown in Fig. 1. The circuit comprises an internal resistance R_0, two RC pairs (R_1, C_1) and (R_2, C_2) representing electrochemical and concentration polarization, and an open-circuit voltage (OCV) source ϕ. The terminal voltage is y, with v_1, v_2 being the RC voltages. The SoC $x_{\mathrm{SoC}} \in [0,1]$ is obtained via Coulomb counting, normalized by the nominal capacity $\bar{Q}$. The input current u is positive for charging and negative for discharging.

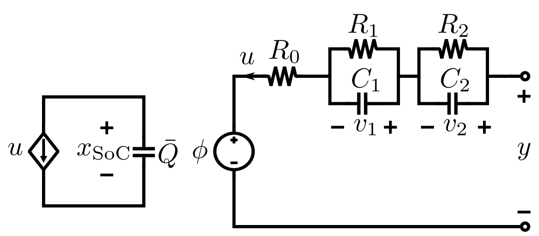

Fig. 1: Second order ECM adopted.

By applying Kirchhoff's current and voltage laws, the voltage–current dynamics of the battery can be expressed in the state-space form given by (1)–(4):

$$\dot{v}_1(t) = -\frac{1}{R_1 C_1} v_1(t) + \frac{1}{C_1} u(t) \tag{1}$$

$$\dot{v}_2(t) = -\frac{1}{R_2 C_2} v_2(t) + \frac{1}{C_2} u(t) \tag{2}$$

$$\dot{x}_{\mathrm{SoC}}(t) = \frac{\eta_Q}{3600\bar{Q}} u(t) \tag{3}$$

$$y(t) = v_1(t) + v_2(t) + R_0 u(t) + \phi(x_{\mathrm{SoC}}) \tag{4}$$

In this model, the parameter η_Q is the Coulombic efficiency, which can normally be calculated as the ratio between discharge and charge capacity, typically being close to unity for a fresh cell. In this work, however, η_Q is treated as an adjustment parameter to be identified in real time, as detailed in Section III.

The OCV function ϕ was selected such that: (i) it depends only on x_{SoC} (neglecting temperature and rate effects); (ii) it is monotonically increasing on $[0,1]$; (iii) it allows the use of the immersion without increasing the system order [15]. The exponential form was adopted:

$$\phi(x_{\mathrm{SoC}}) = \alpha_1 e^{\beta_1 x_{\mathrm{SoC}}(t)} + \alpha_2 e^{\beta_2 x_{\mathrm{SoC}}(t)}. \tag{5}$$

The parameters in (5) are tuned such that one exponential captures the rapid voltage drop observed when the SoC falls below 20%, while the other represents the approximately linear behavior for SoC values above this threshold. The coefficients α_1, α_2, β_1, and β_2 are identified jointly with the ECM parameters R_0, R_1, C_1, R_2, and C_2. The data collection procedure and the identification methodology are described in Section III.

B. Immersion transformation

The objective is to transform the nonlinear system into one with a linear output through an immersion transformation (see [15]). To this end, consider the continuous-time state-space model given by (1)–(4). Let us perform the following change of variables:

$$z_1(t) = \alpha_1 \mathrm{e}^{\beta_1 x_{\mathrm{SoC}}(t)} + \alpha_2 \mathrm{e}^{\beta_2 x_{\mathrm{SoC}}(t)} \tag{6}$$

$$z_2(t) = \alpha_1 \beta_1 \mathrm{e}^{\beta_1 x_{\mathrm{SoC}}(t)} + \alpha_2 \beta_2 \mathrm{e}^{\beta_2 x_{\mathrm{SoC}}(t)} \tag{7}$$

$$z_3(t) = v_1(t) \tag{8}$$

$$z_4(t) = v_2(t) \tag{9}$$

This transformation yields a new system in the z-basis, whose dynamic equations are defined as:

$$\dot{z}_1(t) = \frac{u(t)}{3600Q} z_2(t) \tag{10}$$

$$\dot{z}_2(t) = -\frac{\beta_1 \beta_2 u(t)}{3600Q} z_1(t) + \frac{(\beta_1 + \beta_2) u(t)}{3600Q} z_2(t) \tag{11}$$

$$\dot{z}_3(t) = -\frac{1}{R_1 C_1} z_3(t) + \frac{1}{C_1} u(t) \tag{12}$$

$$\dot{z}_4(t) = -\frac{1}{R_2 C_2} z_4(t) + \frac{1}{C_2} u(t) \tag{13}$$

$$y(t) = z_1(t) + z_3(t) + z_4(t) + R_0 u(t) \tag{14}$$

In this new basis, the model output becomes a linear function of the states, with the original nonlinearity encapsulated in z_1 and z_2. Note that $Q = \bar{Q}/\eta_Q$ incorporates the Coulombic efficiency. Considering the discrete-time model obtained via Euler discretization with sampling period $T_s = 1$ s:

$$z[k+1] = \mathrm{A}(u)\, z[k] + \mathrm{B}_u u[k] \tag{15}$$

$$y[k] = \mathrm{C} z[k] + \mathrm{D}_u u[k], \tag{16}$$

where $z^\top = \begin{bmatrix} z_1 & z_2 & z_3 & z_4 \end{bmatrix}$, and

$$\mathrm{A}(u) = \begin{bmatrix} 1 & T_s b_3 u & 0 & 0 \\ -T_s \beta_1 \beta_2 b_3 u & 1 + T_s b_3 (\beta_1 + \beta_2) u & 0 & 0 \\ 0 & 0 & a_1 & 0 \\ 0 & 0 & 0 & a_2 \end{bmatrix},$$

$$\mathrm{B}_u^\top = \begin{bmatrix} 0 & 0 & b_1 & b_2 \end{bmatrix}, \quad \mathrm{C} = \begin{bmatrix} 1 & 0 & 1 & 1 \end{bmatrix}, \quad \mathrm{D}_u = R_0.$$

with $a_i = -T_s/(R_i C_i)$, $b_i = 1/C_i$ for $i = 1, 2$, and $b_3 = T_s/(3600Q)$. To use this structure, it is necessary to demonstrate the observability characteristics, which can be verified in Subsection 3.2 of [16].

III. Methodological procedures

This section describes the offline parameter identification and real-time estimation framework. Fig. 2 illustrates the overall structure, comprising two layers: offline identification (capacity, OCV, RC parameters via FFRLS) and real-time operation (event-based R_0 estimation, KFLO, and recursive η_Q update).

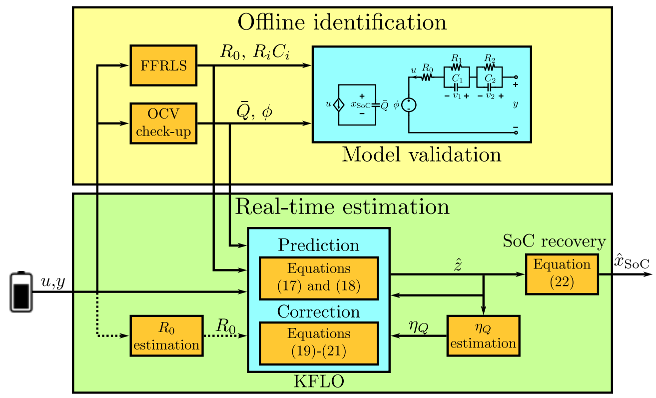

Fig. 2: Schematic diagram showing the process operation, including offline operation and real-time estimation. The dashed line represents an event-driven operation.

A. Offline identification

The identification of both the OCV curve and the ECM parameters was performed on a fresh 3.3 Ah Panasonic NCR18650Ga NMC lithium-ion cell. The cell was placed in a temperature-regulated test chamber maintained at 25°C throughout the experiments. A BioLogic BCS-810 battery cycler was used to impose current profiles and acquire measurements of terminal voltage, current, and cell surface temperature. The cycler is controlled by the BioLogic BT-Lab proprietary software. The offline identification is conducted in a controlled environment before each discharge cycle, updating the model parameters prior to real-time operation.

1) OCV check-up: The OCV curve was characterized via a C/20 test with a full discharge to 2.5 V, full charge, and full discharge, with 5-minute rests between steps. The average of the charge and discharge curves yields the OCV-SoC characteristic. Using MATLAB's Curve Fitting Toolbox, the parameters of (5) were estimated for fresh and aged cells (Table I). Fig. 3(a) shows the fitted curves (RMSE: 0.529% for fresh, 0.236% for aged). The OCV parameters show minimal variation with aging once capacity is updated, justifying offline identification.

TABLE I: Parameters identified for the OCV curve considering both fresh and aged batteries.

Parameters	Fresh	Aged
α_1 (V)	3.3230	3.3863
α_2 (V)	-0.7336	-0.8907
β_1	0.2311	0.2037
β_2	-26.4911	-17.9295
$\bar{Q}$ (Ah)	3.30	2.31

Notably, the OCV curve parameters exhibit minimal variation over the battery's lifespan once the usable capacity is updated, justifying the offline identification of the OCV characteristic in the proposed framework.

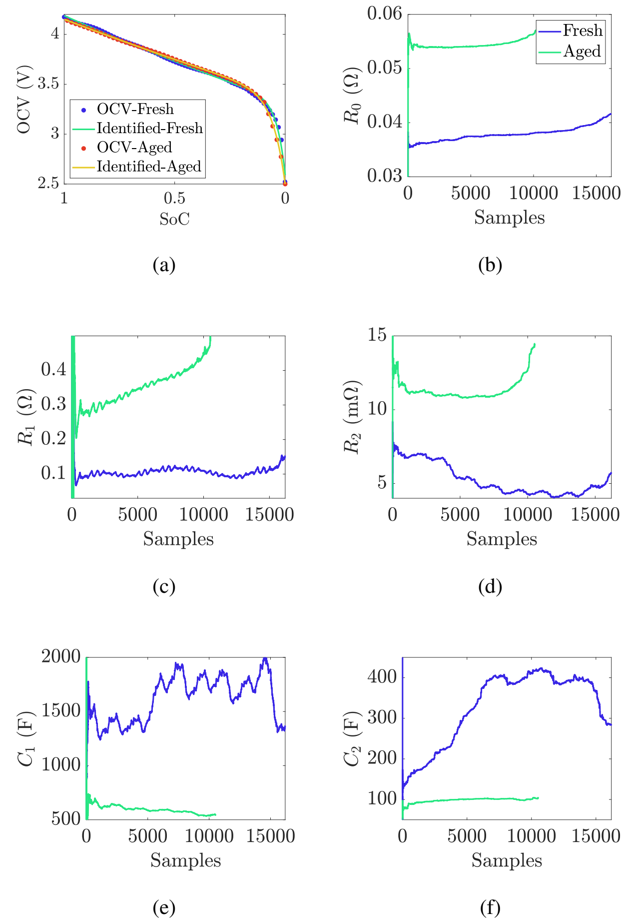

Fig. 3: Curves identified when the FFRLS was applied to the fresh and aged battery for (a) OCV curve, (b) R_0, (c) R_1, (d) R_2, (e) C_1, and (f) C_2.

2) RC parameters identification: A current profile derived from the WLTP Class 3 driving cycle [17] was applied. Parameters were estimated via FFRLS [18], [19]. Figs. 3(b)-(f) show the time evolution of the estimates; the final values (Table II) were obtained by averaging after convergence.

TABLE II: Parameters identified for the ECM model considering both fresh and aged batteries.

Parameters	Fresh	Aged
R_0 (mΩ)	38.0314	54.5499
R_1 (mΩ)	106.0383	357.5534
R_2 (mΩ)	5.1156	11.3093
C_1 (F)	1,632.3429	588.3891
C_2 (F)	339.8752	99.4552

At first glance, clear patterns can be observed. For the aged battery, all resistive elements increase, whereas the capacitive elements decrease. These trends are consistent with the expected physical effects of aging: increased internal losses manifest as higher resistance, while electrode degradation reduces the effective charge storage capacity, reflected in lower capacitance values. R_0 increased by 43%, the R_1C_1

time constant increased by 21%, and the R_2C_2 time constant decreased by 35%, significantly altering the model dynamics.

Remark *1:* Here, R_0 is updated via events. Unlike abstract RC parameters, R_0 has direct physical meaning, is simpler to estimate than capacity, and is useful for health monitoring [20].

B. Real-time estimation

This section presents the real-time estimation framework, comprising three main components: the Kalman filter with linear output (KFLO), the event-based internal resistance estimator, and the recursive update law for the Coulombic efficiency η_Q.

1) Kalman filter with linear output: The discrete model (15)–(16) enables a standard Kalman filter:

$$\hat{z}[k+1,k] = \mathrm{A}(u)\hat{z}[k,k] + \mathrm{B}_u u[k] \tag{17}$$

$$\mathrm{P}[k+1,k] = \mathrm{A}(u)\mathrm{P}[k,k]\mathrm{A}^\top(u) + \mathrm{Q} \tag{18}$$

$$\mathrm{L}[k] = \mathrm{P}[k,k-1]\mathrm{C}^\top(\mathrm{C}\mathrm{P}[k,k-1]\mathrm{C}^\top + \mathrm{R})^{-1} \tag{19}$$

$$\hat{z}[k,k] = \hat{z}[k,k-1] + \mathrm{L}[k](y[k] - \mathrm{C}\hat{z}[k,k-1] - \mathrm{D}_u u[k]) \tag{20}$$

$$\mathrm{P}[k,k] = (\mathrm{I}_4 - \mathrm{L}[k]\mathrm{C})\mathrm{P}[k,k-1](\mathrm{I}_4 - \mathrm{L}[k]\mathrm{C})^\top + \mathrm{L}[k]\mathrm{R}\mathrm{L}^\top[k] \tag{21}$$

SoC is recovered via inverse transformation:

$$\hat{x}_{\mathrm{SoC}}[k] = \frac{1}{\beta_1}\ln\left(\left|\frac{\beta_2\hat{z}_1[k,k] - \hat{z}_2[k,k]}{\alpha_1(\beta_2-\beta_1)}\right|\right) \tag{22}$$

The EKF and UKF were also implemented for comparison. Their gains were tuned by trial and error for optimal fresh-cell performance. The final parameters are summarized in Table III.

TABLE III: Adjusted matrices for the designed estimators.

Structure	$\mathrm{P}[0,0]$	Q	R
KFLO	$\mathrm{diag}\,(1000,1,1,1)$	$10^{-9}\mathrm{I}_4$	11
EKF	$\mathrm{diag}\,(1,1,100)$	$10^{-9}\mathrm{I}_3$	1
UKF	$\mathrm{diag}\,(1,1,0.7)$	$10^{-9}\mathrm{I}_3$	1

2) Event-based internal resistance estimation: The internal resistance estimator is placed before the KFLO algorithm in the processing flow, as its primary function is to provide an updated R_0 value to improve estimation accuracy. The update mechanism is event-driven: let $u[k]$ and $u[k-1]$ denote the current measurements at instants k and $k-1$, respectively. If the current variation $\Delta u = |u[k] - u[k-1]|$ exceeds a predefined threshold δ, the internal resistance is updated using Ohm's law:

$$R_0 = \left|\frac{\Delta y}{\Delta u}\right| = \left|\frac{y[k]-y[k-1]}{u[k]-u[k-1]}\right|, \tag{23}$$

where $y[k]$ and $y[k-1]$ are the corresponding voltage measurements. In this work, the threshold was set to $\delta = 0.4$ A, which empirically provided the best trade-off, ensuring that small variations caused by measurement noise are filtered out while reliably detecting current steps large enough to yield a meaningful resistance estimate. The approach is inspired by the offline identification procedure described in [21], where the instantaneous current variation from a pulsed signal is used to estimate R_0.

3) Coulombic efficiency update: The Coulombic efficiency update is performed after the KFLO, as it relies on the estimated state variables. Discretizing (10) and using the output equation (16), the voltage at instant k can be expressed as a function of η_Q:

$$\hat{y}[k] = \hat{z}_1[k-1] + \frac{\eta_Q}{3600\bar{Q}}u[k-1]\hat{z}_2[k-1] + \hat{z}_3[k] + \hat{z}_4[k] + R_0 u[k], \tag{24}$$

where $\hat{z}_i[k]$, $i = 1,\ldots,4$ denote the estimated states from the KFLO. Equation (24) is linear in the unknown parameter η_Q, allowing its recursive estimation via a Recursive Least Squares (RLS) algorithm. At each time step, the RLS updates $\hat{\eta}_Q$ to minimize the prediction error between the measured voltage $y[k]$ and the predicted $\hat{y}[k]$.

IV. Analysis of performance degradation

This section evaluates the performance degradation of the proposed KFLO estimator compared to the EKF and UKF benchmarks for both fresh and aged cells. Two metrics are employed to quantify estimation accuracy: the Root Mean Square Error (RMSE) and the Mean Absolute Error (MAE), both expressed as percentages:

$$\mathrm{RMSE}_{\%} = 100\sqrt{\frac{1}{N}\sum_{k=1}^{N}\left(\frac{\mathrm{SoC}[k] - \hat{x}_{\mathrm{SoC}}[k]}{\mathrm{SoC}[k]}\right)^2} \tag{25}$$

$$\mathrm{MAE}_{\%} = 100\frac{1}{N}\sum_{k=1}^{N}\left|\frac{\mathrm{SoC}[k] - \hat{x}_{\mathrm{SoC}}[k]}{\mathrm{SoC}[k]}\right|, \tag{26}$$

where N is the number of samples and SoC denotes the reference SoC obtained via Coulomb counting.

We begin the analysis with the fresh battery. Figures 4(a) and (c) show the voltage and SoC estimation results for this case, while the corresponding performance metrics are summarized in Table IV.

In this scenario, the proposed KFLO achieved the lowest voltage estimation errors among all filters, with RMSE and MAE values at least 4.2% and 2.5% lower than those of the EKF and UKF, respectively.

For SoC estimation, the KFLO presented mixed performance. Its RMSE was 0.17% lower than that of the EKF, but 2.2% higher than that of the UKF. However, in terms of MAE, the KFLO outperformed both benchmarks, achieving errors at least 7% lower than those of the EKF and UKF.

We now turn to the aged cell scenario. The same estimators originally tuned for the fresh cell were applied to the aged cell, now benefiting from the real-time correction mechanisms for internal resistance (R_0) and Coulombic efficiency (η_Q) described in Section III. The voltage and SoC estimation results are shown in Figs. 4(b) and (d), with the corresponding performance metrics summarized in Table IV.

In this case, the analysis is divided into two parts. First, we compare the performance of the three estimators (KFLO, EKF, and UKF) when operating on the aged cell. Second, we examine how each estimator's performance degrades relative to its own performance on the fresh cell, providing insight into its robustness to aging.

Comparing the performance of the three estimators on the aged cell, the proposed KFLO consistently outperformed

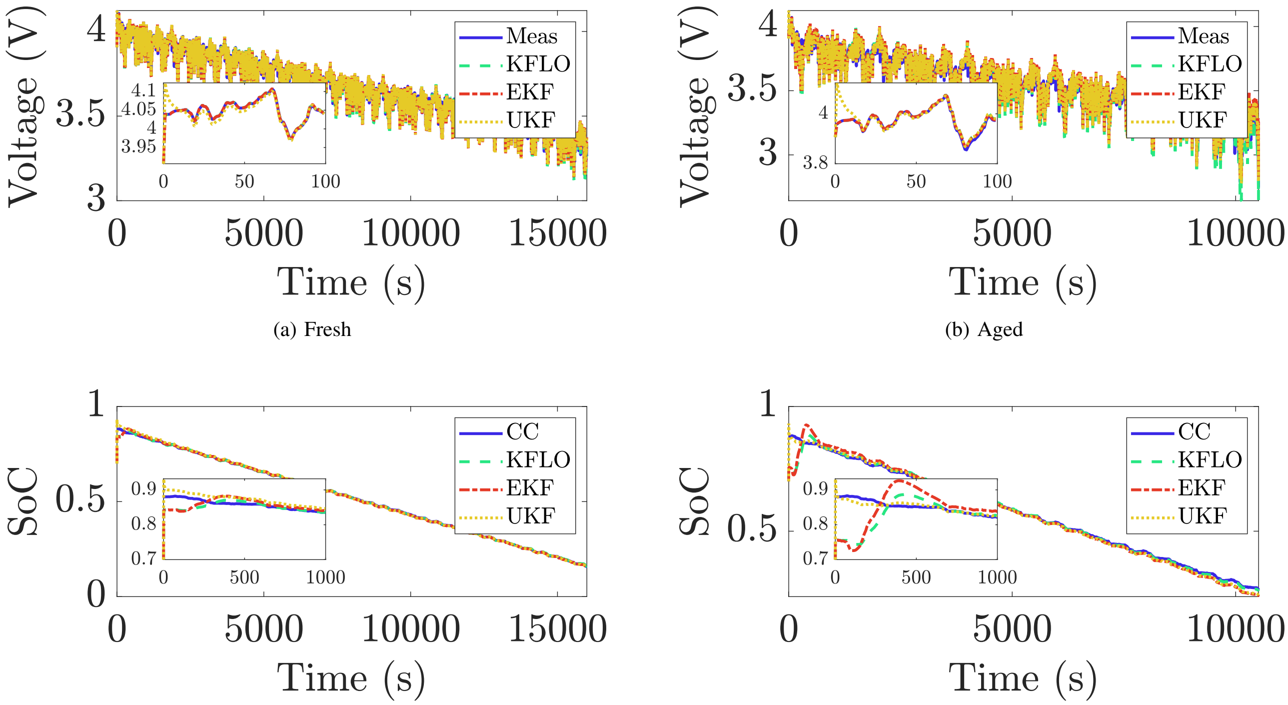

(a) Fresh (b) Aged

(c) Fresh (d) Aged

Fig. 4: Comparative performance among the estimators for voltage and SoC estimation for the battery (a) and (c) Fresh, (b) and (d) Aged.

TABLE IV: Performance comparison among the estimation structures when the battery is fresh and when the battery is aged.

Variable	Structure	Fresh		Aged	
		RMSE	MAE	RMSE	MAE
Voltage	KFLO	0.3811	0.3033	1.1386	0.9067
	EKF	0.4153	0.3237	1.5118	1.1477
	UKF	0.3979	0.3113	1.2293	0.9514
SoC	KFLO	0.6888	0.3782	2.4240	1.2615
	EKF	0.6900	0.4068	3.8050	2.5750
	UKF	0.6742	0.4968	2.5159	1.6491

both the EKF and UKF in terms of voltage and SoC estimation accuracy. For voltage, the KFLO achieved RMSE and MAE values at least 7.3% and 4.6% lower, respectively, than the benchmarks. For SoC estimation, the KFLO obtained RMSE and MAE values at least 3.6% and 23.5% lower than those of the EKF and UKF.

When comparing each estimator's performance on the aged cell against its own performance on the fresh cell, a significant degradation is observed across all methods, even with the real-time correction mechanisms active. Although this degradation is not immediately apparent in the figures, the error metrics reveal increases of more than threefold for voltage estimation and nearly fourfold for SoC estimation.

Among the three estimators, the EKF suffered the most severe degradation, with RMSE and MAE increasing by factors of 5.5 and 6.3, respectively. In contrast, the proposed KFLO exhibited the greatest robustness to aging, with RMSE and MAE increases of only 3.5 and 3.3 times, respectively.

Figure 5 shows the event-based estimates of internal resistance R_0 and Coulombic efficiency η_Q throughout the experiment. Two observations can be drawn from these results.

First, the event-based resistance estimation reveals a consistent pattern: R_0 tends to increase near the end of the charge cycle, as can be seen from the moving average of the instantaneous estimates. This behavior is consistent with the expected increase in internal resistance at low SoC. Second, the estimated η_Q exhibits markedly different dynamics depending on the estimator. While the EKF and UKF yield a relatively steady-state η_Q after an initial transient, the KFLO shows a persistent decrease throughout the cycle.

Furthermore, for all estimators, the variation in η_Q was more visible for the aged cell, confirming that the efficiency correction mechanism becomes increasingly relevant as the battery degrades.

V. Conclusions and Future Works

This paper investigated low-complexity SoC estimator degradation under battery aging, focusing on a novel estimator based on an immersion transformation. The transformation reformulates the nonlinear ECM into a higher-dimensional linear system, enabling a classical Kalman filter with linear output (KFLO). A hybrid framework combines offline parameter estimation with real-time updates of internal resistance (R_0, event-driven) and Coulombic efficiency (η_Q, recursive) to mitigate aging effects.

Experimental results show significant performance degradation with aging for all estimators, despite correction

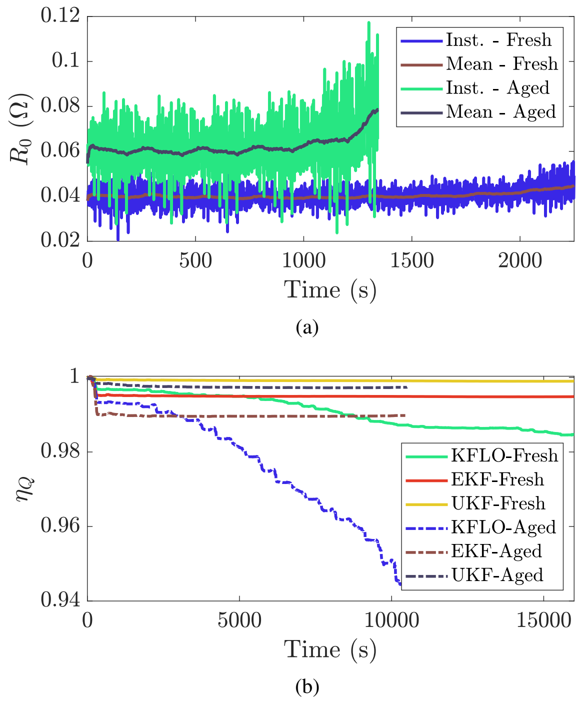

Fig. 5: Update of key model parameters: (a) Event-based internal resistance and (b) Battery capacity coefficient η_Q.

mechanisms. However, KFLO exhibited greater robustness than EKF and UKF, maintaining SoC estimation within acceptable bounds even as the battery approached end-of-life. This resilience suggests that immersion-based linearization combined with event-driven updates effectively compensates for aging variations despite the estimator's simplicity.

The offline identification of RC parameters is currently a limitation of the proposed approach. Future work will address this by enabling online RC updates triggered by significant changes in R_0, or by designing dedicated real-time algorithms to improve estimation accuracy. Moreover, the integration of temperature effects into the model and estimation framework is expected to further improve accuracy under realistic operating conditions. Second, a trigger mechanism for online updating of the RC parameters could enhance the model's adaptability over the battery's lifespan. Finally, the estimated parameters, particularly R_0 and η_Q, may be exploited for joint SoC and SoH estimation, providing a more comprehensive battery health monitoring solution.

Acknowledgment

The authors would like to thank their colleagues Yann BULTEL, Pierre-Xavier THIVEL, and Céline DECAUX, who are with Laboratory of Electrochemistry and Physical-Chemistry of Materials and Interfaces (LEPMI) in Grenoble, France, for their help in defining and programming the battery cycling protocols and carrying out the experiments.

References

[1] C. Ji, D. Liu, Y. Liu, S. Wang, Y. Wang, Z. Zhang, and B. Wang, "Effect of low temperature and high-rate cyclic aging on thermal characteristics and safety of lithium-ion batteries," *Process Safety and Environmental Protection*, vol. 188, pp. 1514–1526, 2024.

[2] Y. Wang, J. Tian, Z. Sun, L. Wang, R. Xu, M. Li, and Z. Chen, "A comprehensive review of battery modeling and state estimation approaches for advanced battery management systems," *Renewable and Sustainable Energy Reviews*, vol. 131, p. 110015, 2020.

[3] M. Khalil, R. Postoyan, and S. Raël, "Systematic observer design with robust global convergence guarantees for a large class of lithium-ion battery models," *IEEE Control Systems Letters*, vol. 9, pp. 649–654, 2025.

[4] M. Saeed, A. Khalatbarisoltani, Z. Deng, W. Liu, F. Altaf, S. Lu, and X. Hu, "Comparative analysis of control observer-based methods for state estimation of lithium-ion batteries in practical scenarios," *IEEE/ASME Transactions on Mechatronics*, vol. 30, no. 5, pp. 3697–3709, 2025.

[5] L. Wildfeuer, A. Karger, D. Aygül, N. Wassiliadis, A. Jossen, and M. Lienkamp, "Experimental degradation study of a commercial lithium-ion battery," *Journal of Power Sources*, vol. 560, p. 232498, 2023.

[6] A. Krupp, R. Beckmann, T. Diekmann, E. Ferg, F. Schuldt, and C. Agert, "Calendar aging model for lithium-ion batteries considering the influence of cell characterization," *Journal of Energy Storage*, vol. 45, p. 103506, 2022.

[7] M. Feinauer, M. Wohlfahrt-Mehrens, M. Hölzle, and T. Waldmann, "Temperature-driven path dependence in li-ion battery cyclic aging," *Journal of Power Sources*, vol. 594, p. 233948, 2024.

[8] P. Guo, W. Ma, X. Liu, and B. Chen, "Robust model parameter identification and soc estimation for li-ion batteries considering noisy measurement," *IEEE Transactions on Industrial Electronics*, vol. 72, no. 11, pp. 11 897–11 907, 2025.

[9] S. Wang, H. Gao, P. Takyi-Aninakwa, J. M. Guerrero, C. Fernandez, and Q. Huang, "Improved multiple feature-electrochemical thermal coupling modeling of lithium-ion batteries at low-temperature with real-time coefficient correction," *Protection and Control of Modern Power Systems*, vol. 9, no. 3, pp. 157–173, 2024.

[10] ——, "Improved multiple feature-electrochemical thermal coupling modeling of lithium-ion batteries at low-temperature with real-time coefficient correction," *Protection and Control of Modern Power Systems*, vol. 9, no. 3, pp. 157–173, 2024.

[11] L. Sun, G. Li, and F. You, "Combined internal resistance and state-of-charge estimation of lithium-ion battery based on extended state observer," *Renewable and Sustainable Energy Reviews*, vol. 131, p. 109994, 2020.

[12] H. Zhang, B. Hu, Z. Yu, H. Wang, L. Qu, DebaoYang, J. Wang, W. Li, C. Bai, and Y. Sun, "State-of-charge estimation of lithium-ion battery based on improved equivalent circuit model considering hysteresis combined with adaptive iterative unscented kalman filtering," *Journal of Energy Storage*, vol. 102, p. 114105, 2024.

[13] I. M. Monirul, L. Qiu, and R. Ruby, "Accurate SOC estimation of ternary lithium-ion batteries by hppc test-based extended kalman filter," *Journal of Energy Storage*, vol. 92, p. 112304, 2024.

[14] S. Wang, S. Zhang, S. Wen, and C. Fernandez, "An accurate state-of-charge estimation of lithium-ion batteries based on improved particle swarm optimization-adaptive square root cubature kalman filter," *Journal of Power Sources*, vol. 624, p. 235594, 2024.

[15] G. Besançon, *Nonlinear Observers and Applications*, ser. Lecture Notes in Control and Information Sciences. Springer Berlin Heidelberg, 2007.

[16] I. Valente de Bessa, G. Besançon, A. I. Bratcu, D. Coutinho, and I. Munteanu, "A linear framework for low-complexity soc estimation in lithium-ion batteries validated with real data," *Control Engineering Practice*, vol. 174, p. 107021, 2026.

[17] I. Munteanu, A. I. Bratcu, G. Besançon, D. Georges, P.-X. Thivel, and Y. Bultel, "Two-level Electrochemical-model-based Estimation of Li-ion Battery State of Charge – Real-data Validation on an Electric Vehicle Use Case," in *2024 IEEE Conference on Control Technology and Applications (CCTA)*, 2024, pp. 268–275.

[18] I. Landau and G. Zito, *Digital Control Systems*, ser. Communications and Control Engineering. Springer London, 10 2005.

[19] Y. Li, H. Guo, F. Qi, Z. Guo, and M. Li, "Comparative Study of the Influence of Open Circuit Voltage Tests on State of Charge Online Estimation for Lithium-Ion Batteries," *IEEE Access*, vol. 8, pp. 17 535–17 547, 2020.

[20] A. Bavand, S. A. Khajehoddin, M. Ardakani, and A. Tabesh, "Online estimations of li-ion battery soc and soh applicable to partial charge/discharge," *IEEE Transactions on Transportation Electrification*, vol. 8, no. 3, pp. 3673–3685, 2022.

[21] Q. Zhu, L. Li, X. Hu, N. Xiong, and G.-D. Hu, "h_∞-based nonlinear observer design for state of charge estimation of lithium-ion battery with polynomial parameters," *IEEE Transactions on Vehicular Technology*, vol. 66, no. 12, pp. 10 853–10 865, 2017.